Enhanced Hemispheric Thermal Contrast Intensified the Indian Monsoon During the Last Interglacial

Kaiqi Chen[1], Qiong Zhang[2], Josefine Axelsson[2], Jianping Li[3,4], Lanning Wang[1]

[1]College of Global Change and Earth System Sciences, Beijing Normal University, Beijing, China.

[2]Department of Physical Geography and Bolin Centre for Climate Research, Stockholm University, Sweden.

[3]Frontiers Science Center for Deep Ocean Multispheres and Earth System (FDOMES)/Key Laboratory of Physical Oceanography/Institute for Advanced Ocean Studies, Ocean University of China, Qingdao 266100, China.

[4]Laboratory for Ocean Dynamics and Climate, Pilot Qingdao National Laboratory for Marine Science and Technology, Qingdao 266237, China.

Corresponding author: Qiong Zhang (qiong.zhang@natgeo.su.se), Jianping Li (ljp@ouc.edu.cn)

Key Points:

- Paleo proxy data and the model simulations indicate an intensified Indian summer monsoon during the last interglacial.
- Orbital forcing during the last interglacial increased the hemispheric thermal gradient and enhanced the land-sea contrast in South Asia.
- The Indian summer monsoon during the last interglacial was further amplified by feedbacks in the equatorial Indian Ocean and Pacific Ocean.

Abstract

Observational data from the past century show a weakening trend in summer monsoon over the Indian subcontinent. This is possibly attributed to the reduced land–sea contrast resulting from the Indian Ocean warming under the rapid increase of greenhouse gases in the atmosphere. In contrast, speleothem records indicate that the Indian summer monsoon was stronger during the last interglacial (LIG) warm period than it is today. Using climate model simulations, we show that orbital forcing effect during the LIG, as well as related ocean feedbacks, led to warming in the Eurasian continent and cooling in the Indian Ocean basin. This amplified the land–sea contrast in the region and intensified the Indian summer monsoon. Although the LIG is often portrayed as a potential analogue of future climate, our study shows that the Indian monsoon responded differently to the LIG warming period than it does to current climate warming.

Plain Language Summary

One way to understand the future climate changes is to learn from the past warm periods. In this case the Last Interglacial (LIG) is often referred as a potential analogue. However, the paleoclimate proxy data such as the speleothem records show a stronger Indian summer monsoon (ISM) in the LIG, in contrast to an observed weakening trend in ISM in past century. In this study we use the climate model simulations to explain why the opposite changes happened in ISM during LIG and current global warming. The warming in the LIG was caused by changed distribution of solar radiation over the earth, which is different to the current warming resulted from increased Greenhouse Gas concentration in the atmosphere. The changes in Indian monsoon are mainly determined by the land-sea contrast in the region. Due to its special geographical location, i.e., north-south orientations of land-sea distribution, the solar radiation changes in LIG enhanced the land-sea contrast and thus intensified the summer monsoon. We suggest that although the LIG is often portrayed as a potential analogue for future climate change, the analogy does not hold in the Indian monsoon region.

1 Introduction

As one of the most powerful tropical monsoon climate systems in the world, the Indian summer monsoon (ISM) can bring moisture from the Indian Ocean towards the continent, resulting in heavy precipitation (Buckley et al., 2014). Even small changes in precipitation over the Indian subcontinent could have significant consequences for agricultural production and socio-economic development (Gadgil & Kumar, 2006; Singh et al., 2014; Vittal et al., 2020). Previous studies have shown that changes to the ISM are highly sensitive to global warming (Kitoh et al., 2013). The frequency of moderate precipitation events and the strength of summer monsoon over the Indian subcontinent have exhibited a significant weakening trend over the past century (Goswami et al., 2006; Li & Zeng, 2002). Meanwhile, global warming has caused sea surface temperature (SST) in the tropical eastern Indian Ocean to rise, which has resulted in a weakening of the land–sea thermal gradient and reduced Indian summer monsoon precipitation (Dinezio et al., 2020; Ramesh & Goswami, 2007; Roxy et al., 2015). Climate models participating in the fifth Climate Model Intercomparison Project (CMIP5) show a large uncertainty in their projections of the Indian monsoon system (Saha et al., 2014). It has been suggested that past warm climates could be used as a potential analogue to understand future climate changes. As part of CMIP, the Paleoclimate Model Intercomparison Project (PMIP) aims to evaluate the ability of CMIP6 models to reproduce past climate by comparing with paleoclimate proxy-data

records and to further our understanding of regional responses to a warmer climate, such as changes in the Indian monsoon (Harrison et al., 2015; Hirabayashi et al., 2013).

The most recent warm period is the last interglacial (LIG), which lasted from 129 to 116 thousand years (ka) before present. During the LIG, the geographical setting and concentration of greenhouse gases (GHGs) in the atmosphere were almost the same as in the present day. The main difference was the incoming solar radiation caused by changes in the Earth's orbit. The global mean surface air temperature was ~2 ℃ higher than in the CMIP6 piControl for 1850 CE (PI) (Hoffman et al., 2017; Turney et al., 2020), and surface temperatures in the northern middle and high latitudes were about 2–5 ℃ higher (Turney & Jones, 2010). These global and hemispheric warming features are similar to projections of future global warming (Otto-Bliesner et al., 2017). The signal of long-term precipitation changes in the Indian monsoon have been mostly recorded in marine sediments and cave deposits (Cai et al., 2015; Cheng et al., 2016; Midhun et al., 2018). The δ18O signal recorded in stalagmites is one of the most important water tracers, but it has given conflicting results regarding changes in Asian monsoon precipitation. Previous studies have combined stalagmite $\delta^{18}O$, $\delta^{44}Ca$, and elemental ratios (e.g., Mg/Ca, Sr/Ca, and Ba/Ca) and shown that the ISM was unstable during the LIG (Magiera et al., 2019). Some other proxy records also showed varied changes in the Asian monsoon (Wang et al., 2008). One reason for this is that the variation in $\delta^{18}O$ is affected by large-scale atmospheric dynamics more than by regional precipitation (Li, 2018; Tan, 2014).

The LIG has been one of the main target periods in PMIP since PMIP3 (Masa et al., 2018). Multiple model ensembles show that there is a significant warming in almost all continents during boreal summer (Lunt et al., 2013; Nikolova et al., 2013; Pedersen et al., 2017). The increased Indian summer monsoon precipitation observed during the LIG contrasts with the decreased Indian summer monsoon precipitation projected under continuous global warming (Turner & Annamalai, 2012). Scussolini et al.(2019) note that the significant increase of Indian summer monsoon precipitation during the LIG period is consistent with the increase of cloud cover and surface cooling. However, there is still a large gap in our understanding of the dynamics of Indian summer monsoon precipitation during the LIG period compared with the Holocene and the present (Han et al., 2019; Lechleitner et al., 2017; Sinha et al., 2015). Current global warming has provided an important impetus to study climatology at higher global temperatures. Understanding the dynamics of ISM precipitation during the LIG will also provide a strong scientific basis for predicting spatiotemporal changes in the Indian climate.

Here we use simulations from the global coupled climate model EC-Earth3 and analyze climatic changes in the ISM region by comparing with a PI control experiment. We find that due to the effect of orbital forcing, Indian summer monsoon precipitation during the LIG increased significantly over the west coast of the Western Ghats and the southern Higher Himalayas but decreased over the equatorial eastern Indian Ocean. These changes in Indian summer monsoon precipitation resulted primarily from enhancement of the hemispheric thermal contrast by changes in orbital forcing, which amplified the land–sea contrast. Meanwhile, the thermal imbalance between the Northern and Southern hemispheres led to an SST anomaly in the Pacific Ocean, which influenced the SST in the eastern Indian Ocean through ocean–atmosphere interactions, enhanced the land–sea contrast over the region, and further intensified the ISM precipitation over the Indian continent.

111 ## 2 Model simulations and methods

112 ### 2.1 EC-Earth model and setup

113 In this study, we use the PMIP4/CMIP6 simulations of the last interglacial and preindustrial
114 period performed by EC-Earth3-LR (Zhang et al., 2021) . EC-Earth is a fully coupled Earth
115 system model that is developed by a European consortium of around 30 research institutions and
116 is widely used in various studies on climate change (Hazeleger et al., 2010, 2012). The
117 atmospheric component of EC-Earth3 is the Integrated Forecasting System model (cycle 36r4)
118 of the European Center for Medium-Range Weather Forecasts (ECMWF), which contains the
119 land surface Hydrology Tiled ECMWF Scheme for Surface Exchanges over Land (Balsamo et
120 al., 2009). The ocean model is the Nucleus for European Modeling of the Ocean (NEMO;
121 Madec, 2008), coupled with the dynamic–thermodynamic sea-ice model Louvain-la-Neuve
122 version 3 (LIM3; Vancoppenolle et al., 2012). Atmospheric-land and ocean-sea-ice components
123 are coupled through the Ocean, Atmosphere, Sea Ice, Soil coupler (Craig et al., 2017). The
124 horizontal resolution of the atmosphere and land is 125 km with 62 vertical layers in the
125 atmosphere; the ocean model, NEMO, has a horizontal resolution of 110 km with 75 vertical
126 layers.

127 We have run the lig127k and piControl simulations following the PMIP4/CMIP6 protocol
128 (Kageyama et al., 2018). The piControl and lig127k have the same boundary conditions expected
129 for the orbital forcing and GHGs. A detailed description of the piControl and lig127k simulations
130 with EC-Earth3-LR is given in Zhang et al. (2021). The orbital forcing is calculated internally in
131 the model. The orbital parameters are set for 1850 CE in the piControl run and for 127 ka before
132 present in the lig127k run (the present day is set as 1950 CE in the orbital parameter calculation).
133 The CO_2, CH_4, and N_2O concentrations in the atmosphere are 284.3 ppm, 808.2 ppb, and 283
134 ppb in the piControl run and 275 ppm, 586 ppb, and 255 ppb in the lig127k run. The lig127k
135 simulation starts from the PI initial conditions and has a spin-up time of about 200 years. The
136 simulation is run for 200 years after reaching equilibrium (i.e., when the global mean
137 temperature trend is less than 0.05 K per century). We use 200 years of data for the analysis.

138 ### 2.2 Statistical methods and indices

139 To investigate changes to the Indian summer monsoon during the LIG, we use a unified
140 dynamical normalized seasonality (DNS) monsoon index defined by Li & Zeng (2002). This
141 index represents the intensity of the monsoon based on the wind field rather than precipitation. It
142 has been shown that this index represents the seasonal cycle and interannual variability of the
143 monsoon over various areas well, especially in Asia (Wang et al., 2008). The index has also been
144 adopted by the National Oceanic and Atmospheric Administration (http://www.cpc.
145 noaa.gov/products/Global_Monsoons/Asian_Monsoons).

146 The DNS index is given by

$$\delta_{nm} = \frac{||\bar{\boldsymbol{V}}_{\boldsymbol{winter}} - \boldsymbol{V}_{\boldsymbol{nm}}||}{||\bar{\boldsymbol{V}}||}, \quad (1)$$

$$\bar{\boldsymbol{V}} = (\bar{\boldsymbol{V}}_{\boldsymbol{winter}} + \bar{\boldsymbol{V}}_{\boldsymbol{summer}})/2, \quad (2)$$

where $\overline{\boldsymbol{V}}_{\boldsymbol{winter}}$ and $\overline{\boldsymbol{V}}_{\boldsymbol{summer}}$ are the climatological winter and summer reference state wind vectors and $\boldsymbol{V}_{\boldsymbol{nm}}$ is the wind vector in a given month. Here, January represents winter and July represents summer. The norm ||A|| is defined as

$$||A|| = (\iint_S |\mathrm{A}|^2 \, \mathrm{dS})^{1/2}, \tag{3}$$

where S denotes the domain of integration. In calculations at a point (*i, j*),

$$||A_{i,j}|| \approx \Delta S[(\left|A_{i-1,j}^2\right| + 4\left|A_{i,j}^2\right| + \left|A_{i+1,j}^2\right|)\cos\varphi_j + \left|A_{i,j-1}^2\right|\cos\varphi_{j-1} + \left|A_{i,j+1}^2\right|\cos\varphi_{j+1}]^{1/2}, \tag{4}$$

where $\Delta S = a\Delta\varphi\Delta\lambda/4$, φ_j is the latitude at the point (*i, j*), $\Delta\varphi$ and $\Delta\lambda$ are resolutions in the meridional and zonal directions, respectively, and a is the mean radius of the Earth (Li & Zeng, 2000).

We compute the DNS monsoon index using the monthly mean wind field at 850 hPa from the PI and LIG simulations.

3 Paleo proxy evidence for an intensified Indian summer monsoon during the LIG

Paleo proxy records indicate that South Asia was wetter during the LIG than in the PI period, mainly because of differences in orbital forcing and higher Northern Hemisphere summer insolation (Liu et al., 2020; Scussolini et al., 2019). Speleothem records from Bittoo cave (Khatayat et al., 2016) and Mawmluh cave (Magiera et al., 2019) both show more depleted oxygen isotopes during Marine Isotope Stage 5e (MIS-5e) than before or after (Fig. 1). Bittoo cave is situated on the edge of the ISM region in northern India (30°47′ 25″N, 77°46′ 35″E) and receives ~80% of its annual precipitation during the monsoonal months of June–September (Khatayat et al., 2016). Mawmluh cave is located in northeastern India (25°15′44″N, 91°52′54″E) and gets 75% of its precipitation during the ISM. The main moisture source for monsoonal precipitation at both cave sites is the Bay of Bengal. Orographic lifting due to the Meghalaya Plateau and strong southeasterly flow over central India leads to extreme monsoon precipitation in this part of the ISM region, especially in northeast India (Magiera et al., 2019).

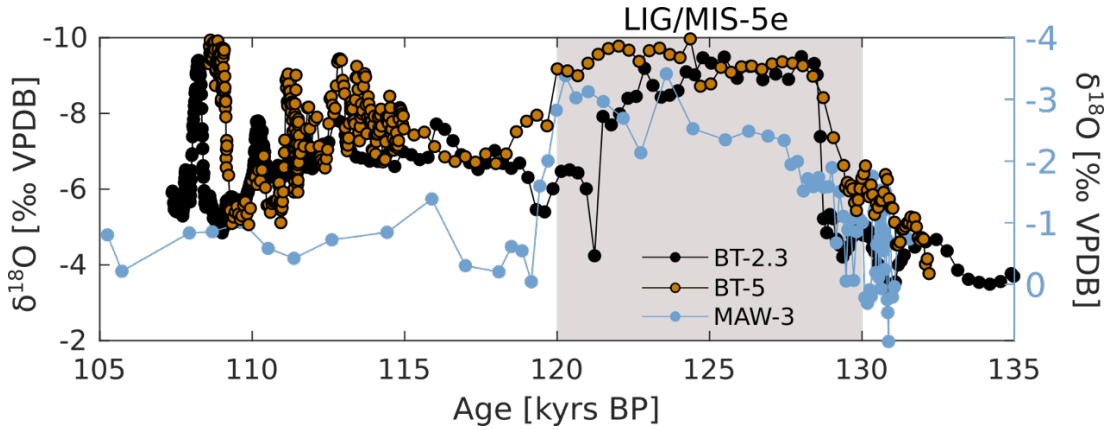

Figure 1. Proxy time-series of $\delta^{18}O$ from Bittoo Cave (BT-2.3: black, BT-5: black/orange) and Mawmluh Cave (MAW-3: blue). Data presented in ‰ relative to VPDB (Vienna Pee Dee Belemnite) standard. LIG/MIS-5e is shaded in grey.

Magiera et al. (2019) also investigated other proxies besides $\delta^{18}O$. Using a combination of $\delta^{18}O$, $\delta^{44}Ca$, and elemental measurements, the authors concluded that the wettest period was between 135 and 100 ka before present, corresponding to the LIG/MIS-5e. The decrease in oxygen isotopes found in the speleothem at both Bittoo cave and Mawmluh cave suggests a stronger ISM with a more remote moisture source than the periods before and after the LIG. Proxy-record evidence of increased monsoon precipitation has also been found for the East Asian summer monsoon, suggesting that the two monsoon systems have a coupled response to changes in orbital forcing (Liu et al., 2020; Scussolini et al., 2019).

4 Enhanced land–sea contrast due to orbital forcing

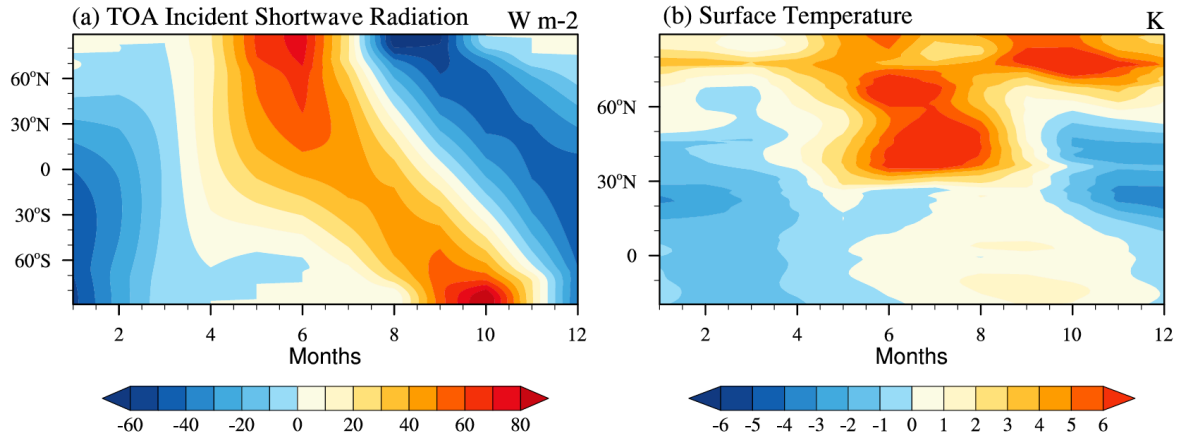

Figure 2. Differences between the LIG and PI periods (LIG minus PI, the same in other figures) in (a) zonal mean TOA insolation and (b) surface temperature, averaged over 50°E–100°E.

Differences in the Earth's orbital parameters (the perihelion, obliquity, and eccentricity) during the LIG led to differences in the seasonal and latitudinal distribution of solar radiation received at the top of the atmosphere (TOA) compared with PI conditions (Berger & Loutre, 1991; Otto-Bliesner et al., 2017). The incoming solar radiation received by the Northern Hemisphere (calculated as the zonal mean over 0°N–90°N) increased by 20.8 W/m^2 from June to September

(JJAS) during the LIG period, which is 7.1% more than that during the PI period (Fig. 2a). The increase in insolation was larger in the Northern Hemisphere than in the Southern Hemisphere, leading to an even larger hemispheric thermal gradient. This contrasts with the current global warming situation, where the growth rate of atmospheric internal energy in the Southern Hemisphere is higher than in the Northern Hemisphere (Chen et al., 2020).

Increased solar radiation at the TOA directly affects the amount of heat reaching the surface and changes the surface energy budget. With increased incoming solar radiation in summer, the warming amplitude over land is larger than that over the ocean and this land–sea contrast triggers the onset of the monsoon. During the LIG, the orbital forcing induced surface warming over both land and ocean, but the warming amplitude was larger over the land than over the ocean (Fig. 2b). The surface temperature of West Asia increased by ~3.6 °C in JJAS, whereas the surface temperature of the northern Indian Ocean increased by only 0.6°C (Fig. 2b). We calculate the land–sea contrast by taking the temperature difference between the Eurasian continent (10°N–90°N, 50°E–100°E) and the Indian Ocean (30°S–10°N and 50°E–100°E). The land–sea contrast in the PI period was 10.4 °C over the Indian monsoon region, but during the LIG it was ~3 °C larger. In other words, the land–sea contrast was enhanced by ~28% during the LIG compared with the PI period.

An increase in the land–sea thermal contrast should enhance the monsoon and lead to more monsoon precipitation (Chou, 2003; Wu et al., 2012). Previous studies have shown an increase in precipitation in the Indian subcontinent during the LIG period, indicating an enhanced monsoon (Magiera et al., 2019; Montoya et al., 2000). Here we quantify the differences in the intensity of the ISM between the LIG and PI periods using the DNS method proposed by Li & Zeng (2002). The DNS index indicates that the average intensity of the ISM during the LIG was 38% larger than during the PI period (not shown).

In summary, during the LIG, the land–sea thermal contrast was 28% larger than during the PI period and the DNS monsoon index was 38% larger. The enhancement of the monsoon and land–sea contrast resulted directly from the differences in insolation. We show below that other indirect impacts further amplified the land–sea contrast and monsoon intensity.

5 Local response to orbital forcing

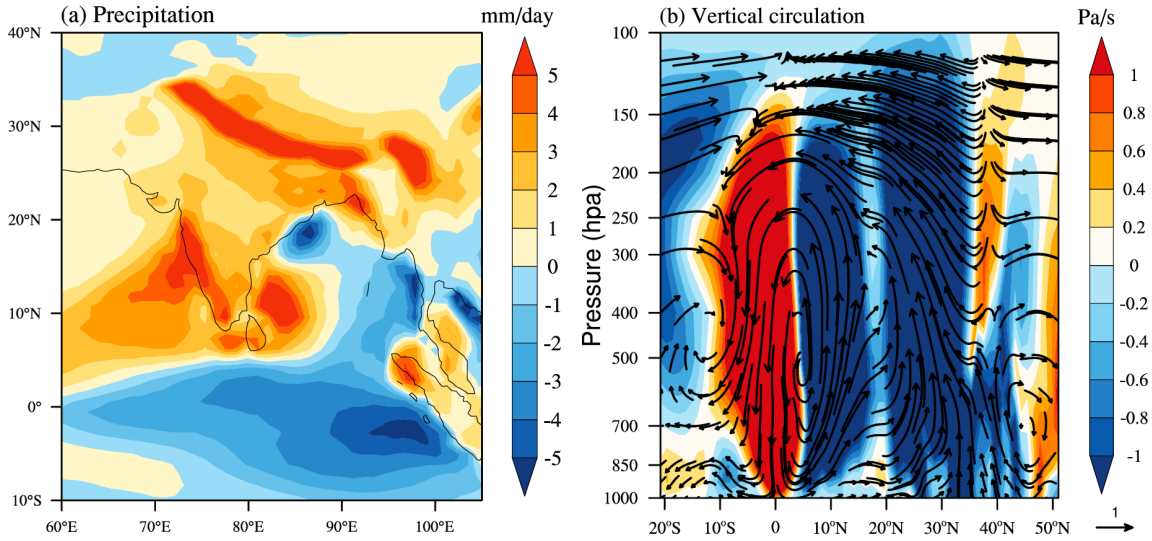

Figure 3. Differences between the LIG and PI periods in (a) precipitation and (b) vertical circulation averaged over 60°E–100°E.

Turner & Annamalai (2012) note that under current GHGs forcing, although the increased land–sea contrast and water vapor should theoretically exacerbate monsoon precipitation, observational results do not provide any cogent evidence for such a positive trend, and even suggest a negative trend. This phenomenon may be related to the complex dynamical feedbacks within the tropical Indo-Pacific region. In contrast, during the LIG warm period, there was a significant increase of ~28% in Indian summer monsoon precipitation compared with the PI period. The major changes in precipitation were prominent in three areas: increased precipitation on the south side of the Himalayas and on the west side of the Western Ghats, and reduced precipitation over the equatorial eastern Indian Ocean (Figure 3a).

The changes in the vertical circulation (Fig. 3b) correspond well to the changes in Indian monsoon precipitation (Fig. 3a). Two prominent local Hadley circulations resemble a "Double-Wall" structure. The ascending air flow near 10°N and 30°N is within the Indian subcontinent and corresponds to the high precipitation centers shown in Fig. 3a. The descending branch is located in the equatorial region around 10°S–5°N and corresponds to the reduced precipitation in the equatorial eastern Indian Ocean. This suggests that the monsoonal flow carried water vapor northward from the Indian Ocean, resulting in strong convection when the topographic barrier was reached. The relationship between the precipitation anomaly pattern and the topography emphasizes the influence of topography and the vertical atmospheric motion on precipitation (Bookhagen & Burbank, 2006; Sudharsan et al., 2020). External forcing, such as the orbital forcing during the LIG, could have resulted in an anomalous near-surface cyclone over the Tibetan Plateau (see Fig. 5a in next section), leading to anomalous upward flow. This might have strengthened the ISM and been conducive to the transport of water vapor from the Bay of Bengal and the Arabian Sea to the Indian subcontinent. The external forcing might also have further amplified the "pumping" effect over the Tibetan Plateau in summer (Wu et al., 2015).

6 Ocean feedbacks and remote forcing from the Pacific

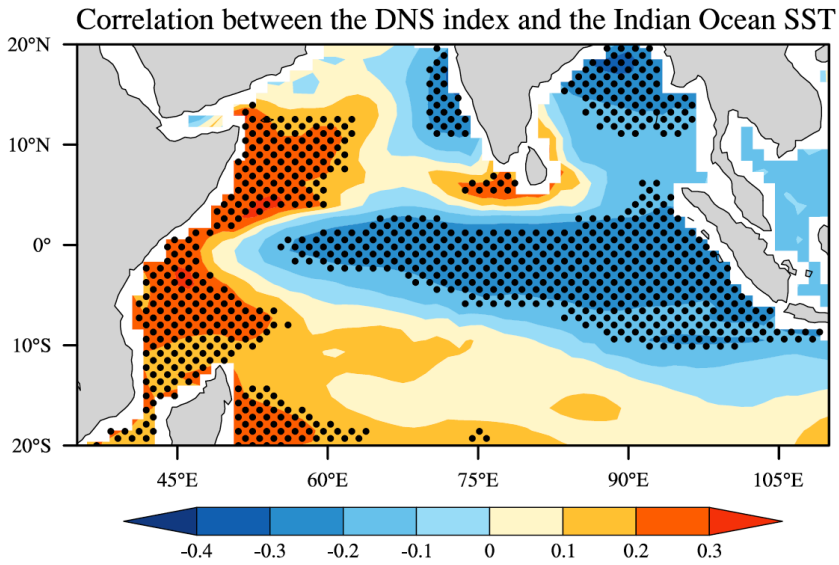

Figure 4. Correlation between the DNS index and the Indian Ocean SST in JJAS during the LIG period. The correlation is calculated using 100 years of data from the EC-Earth3-LR LIG simulation. The stippled area indicates statistical significance at the 0.05 level.

Saji et al. (1999) showed that the tropical Indian Ocean SST has an important influence on the Indian summer monsoon. Figure 4 shows the correlation between the intensity of the Indian summer monsoon (as measured by the DNS index) and the tropical Indian Ocean SST in the LIG period. The conventional monsoon index based on precipitation is primarily statistical, whereas the DNS method, by taking the wind field into account, is more strongly grounded in atmospheric dynamics and describes regional circulations more clearly and accurately (Li et al., 2010; Zhang et al., 2018). Figure 4 shows that there was a statistically significant correlation between the equatorial Indian Ocean SST and the DNS index during the LIG. The correlation exhibits a dipole pattern, with negative correlations in the eastern part of the equatorial Indian Ocean and positive correlations in the western part.

This correlation pattern resembles the SST differences between the LIG and PI periods (Fig. 5a). During the LIG, there was a cold tongue in the eastern equatorial Indian Ocean, with the largest part lying in the Southern Hemisphere. The increased insolation during the LIG (Fig. 2a) did not prevent the formation of this cold tongue and the strong seasonal hemispheric thermal contrast. The cooling might have been associated with the enhancement of the Indian summer monsoon, as shown in Fig. 5a. Bollasina & Ming (2013) showed that the spatial expansion of the Indian Ocean SST mode can affect ocean convection through the modulation of the atmospheric meridional circulation. Such an SST pattern increased the meridional SST gradient in the equatorial Indian Ocean during the LIG. The air on the west side was warmed and rose up whereas on the east side it was cooled and sunk down, thus strengthening the anomalous easterly winds at the surface of the equatorial Indian Ocean.

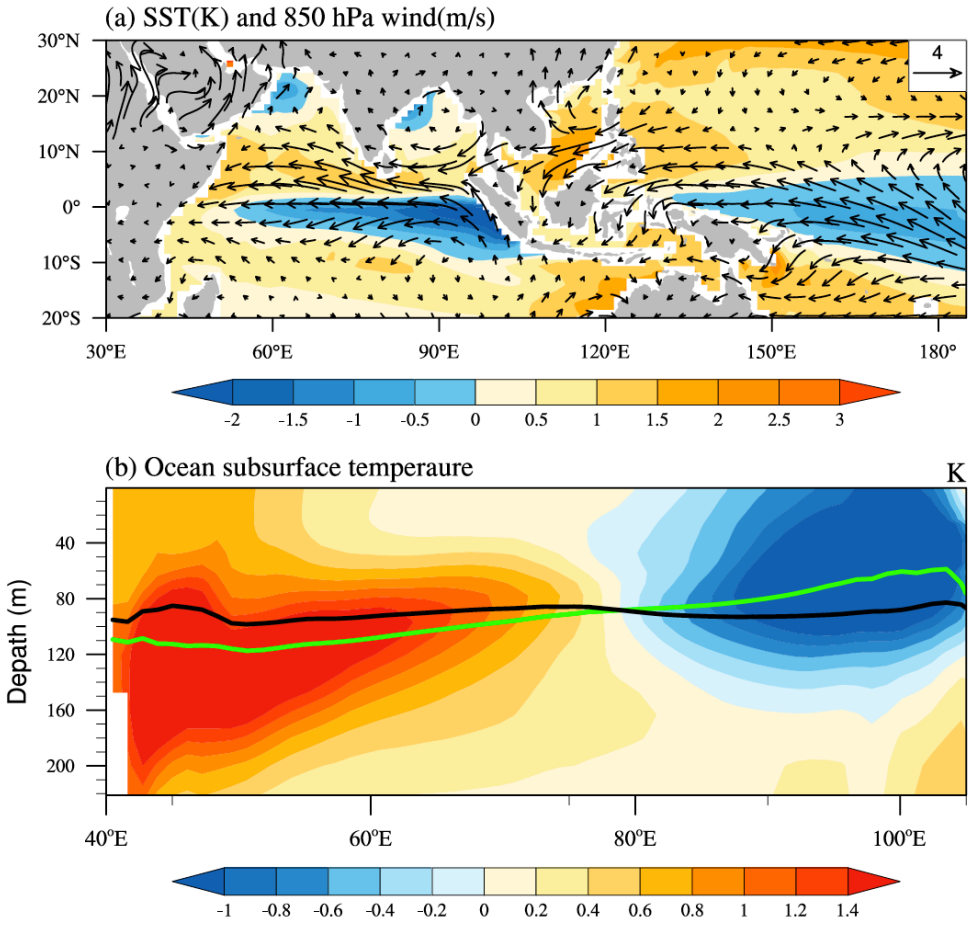

Figure 5. Differences between the LIG and PI periods in (a) 850 hPa wind (vectors), sea surface temperature (shading), and (b) ocean subsurface temperature, averaged over 10°S–5°N. The green line in (b) indicates the thermocline (represented by 23°C isotherm) during the LIG, and the black line indicates the thermocline in the PI period.

Furthermore, the Pacific Ocean can establish a connection with the tropical Indian Ocean through atmospheric circulation (Terray et al., 2021; Tokinaga et al., 2012), which can contribute to the generation of anomalous easterly winds. In addition to the hemispheric thermal contrast in the Indian Ocean in JJAS, there was a strong SST gradient between the northern and southern Pacific Ocean (Fig. 5a). As the SST increased in the North Pacific, the air mass warmed and sunk over the cold SST in the South Pacific, creating a meridional Hadley Circulation over the Pacific Ocean (not shown). Due to the leftward geostrophic deflection in the Southern Hemisphere, the downdrafts were deflected westward over the sea surface, forming anomalous easterly winds over the equatorial western Pacific and Indo-Pacific Warm Pool. According to ocean–atmosphere coupling theory (Bjerknes, 1969), the upwelling of the equatorial eastern Indian Ocean was enhanced under the action of the anomalous easterly winds. As the thermocline became shallower (deeper) in the equatorial eastern (western) Indian Ocean, the SST formed a dipole corresponding to the "warm West and cold East" pattern (Figure 5b). In addition, with the expansion of the SST cooling area in the equatorial eastern Indian Ocean, the land–sea thermal gradient in South Asia was further increased, which had a positive feedback effect on the Indian summer monsoon precipitation.

7 Conclusions

Based on the EC-Earth3-LR model, this work explored whether the LIG could act as a potential analogue of the Indian monsoon system under global warming. Warming in the LIG was caused by different external forcing to current global warming; GHGs are the main external forcing of current warming, whereas orbital forcing drove the hemispheric thermal contrast during the LIG. We found that the Indian summer monsoon was intensified by the orbital forcing during the LIG, which is in contrast to the weakening of the monsoon that has occurred under GHGs forcing. We discussed the physical mechanisms behind the enhanced Indian summer monsoon from two perspectives: the direct effect of the land–sea contrast and the further amplification through ocean feedbacks.

The direct effect of orbital forcing during the LIG enhanced the land–sea contrast in the Indian monsoon region by imposing a stronger hemispheric thermal gradient. The enhanced monsoon flow facilitated the “pumping effect" around the Tibetan Plateau and brought more water vapor from the Indian Ocean to the Indian subcontinent. Meanwhile, two anomalous meridional Hadley circulation structures were formed through topographic uplift, leading to increased precipitation on the coast of the Western Ghats and on the south side of the Himalayas, and a significant decrease in precipitation in the equatorial eastern Indian Ocean. Furthermore, the hemispheric thermal contrast formed anomalous easterly winds in the equatorial eastern Indian Ocean. A similar mechanism in the western Pacific resulted in anomalous easterly winds, which further enhanced the easterly winds in the eastern Indian Ocean. The weakened westerly winds led to a shallower thermocline in the equatorial eastern Indian Ocean and the subsequent upwelling enlarged the cooling area of the sea surface. A cooler eastern Indian Ocean further increased the thermal gradient between the Eurasian continent and the northern Indian Ocean, thus enhancing the Indian summer monsoon. The results indicate that during the LIG, the different insolation from today caused by orbital forcing enhanced the Indian summer monsoon, and this effect was further amplified by the ocean feedbacks in the eastern Indian Ocean and the western Pacific.

In summary, unlike the weakening of the monsoon caused by GHGs warming, the warming during the LIG enhanced the interhemispheric thermal gradient, which strengthened the Indian summer monsoon. This mechanism is specific to the Indian monsoon, where the land–sea contrast is in the north–south direction. The hemispheric thermal contrast may not affect the West African monsoon or the East Asian monsoon, where the land–sea contrast is in the west–east direction. We expect that the mechanisms behind the response of the Indian summer monsoon to orbital forcing during the LIG revealed in this paper will be of substantial and practical value for understanding past climate variability in South Asia and for interpreting future climate change.

Acknowledgements and Data Availability Statement

This work was supported by the Swedish Research Council (Vetenskapsrådet, grant no. 2013-06476 and 2017-04232) and National Natural Science Foundation of China (NSFC) Project (41790474, 41530424) and Shandong Natural Science Foundation Project (ZR2019ZD12), and the Fundamental Research Funds for the Central Universities (201962009). The EC-Earth simulations were performed on ECMWF's computing and archive facilities. Additional resources were provided by the Swedish National Infrastructure for Computing (SNIC) at the National Supercomputer Centre (NSC) partially funded by the Swedish Research Council through grant

agreement no. 2018-05913. The model simulation data are available at the website https://esgf-data.dkrz.de/search/cmip6-dkrz.

The model simulations analysed in this study are distributed and made freely available through the Earth System Grid Federation (ESGF). The PI simulations are available at https://doi.org/10.22033/ESGF/CMIP6.4847 (EC-Earth Consortium (EC-Earth), 2019). The LIG simulations are available at https://doi.org/10.22033/ ESGF/CMIP6.4798 (EC-Earth Consortium (EC-Earth), 2020).

Details on the ESGF can be found on the website of the CMIP panel (https://www.wcrp-climate.org/wgcm-cmip/wgcm-cmip6). The reconstruction data used for data–model comparison is in the Supplement.

References

Balsamo, G., Viterbo, P., Beljaars, A., van den Hurk, B., Hirschi, M., Betts, A. K., & Scipal, K. (2009). A revised hydrology for the ECMWF model: Verification from field site to terrestrial water storage and impact in the Integrated Forecast System. *Journal of Hydrometeorology*, *10*(3), 623. https://doi.org/10.1175/2008JHM1068.1

Berger, A., & Loutre, M.-F. (1991). Insolation values for the climate of the last 10 million years. *Quaternary Science Reviews*, *10*(4), 297-317. https://doi.org/10.1016/0277-3791(91)90033-Q

Bjerknes, J. (1969). Atmospheric teleconnections from the equatorial Pacific. *Monthly Weather Review*, *97*(3), 163-172. https://doi.org/10.1175/1520-0493(1969)0972.3.CO;2

Bollasina, M. A., & Ming, Y. (2013). The general circulation model precipitation bias over the southwestern equatorial Indian Ocean and its implications for simulating the South Asian monsoon. *Climate dynamics*, *40*(3), 823-838. https://doi.org/10.1007/s00382-012-1347-7

Bookhagen, B., & Burbank, D. W. (2006). Topography, relief, and TRMM‐derived rainfall variations along the Himalaya. *Geophysical Research Letters*, *33*(8), 153-172. https://doi.org/10.1029/2006GL026944

Buckley, B. M., Fletcher, R., Wang, S.-Y. S., Zottoli, B., & Pottier, C. (2014). Monsoon extremes and society over the past millennium on mainland Southeast Asia. *Quaternary Science Reviews*, *95*(7) , 1-19. https://doi.org/10.1016/j.quascirev.2014.04.022

Cai, Y., Fung, I. Y., Edwards, R. L., An, Z., Cheng, H., Lee, J.-E., et al. (2015). Variability of stalagmite-inferred Indian monsoon precipitation over the past 252,000 y. *Proceedings of the National Academy of Sciences*, *112*(10), 2954-2959. https://doi.org/10.1073/pnas.1424035112

Chen, K., Li, J., Xie, T., Wang, Q., & Wang, L. 2020. Analysis of the Spatiotemporal Characteristics and Trends of Global Atmospheric Energy. *Chinese Journal of Atmospheric Sciences (in Chinese)*, *44*(1): 168-182. https://doi.org/10.3878/j.issn.1006-9895.1903.18252

Cheng, H., Edwards, R. L., Sinha, A., Spötl, C., Yi, L., Chen, S., et al. (2016). The Asian monsoon over the past 640,000 years and ice age terminations. *Nature*, *534*(7609), 640-646. https://doi.org/10.1038/nature18591

Chou, C. (2003). Land–sea heating contrast in an idealized Asian summer monsoon. *Climate Dynamics*, *21*(1), 11-25. https://doi.org/10.1007/s00382-003-0315-7

Craig, A., Valcke, S., & Coquart, L. (2017). Development and performance of a new version of the OASIS coupler, OASIS3-MCT_3.0. *Geoscientific Model Development*, *10*(9), 3297-3308. https://doi.org/10.5194/gmd-2017-64

Dinezio, P. N., Puy, M., Thirumalai, K., Jin, F.-F., & Tierney, J. E. (2020). Emergence of an equatorial mode of climate variability in the Indian Ocean. *Science Advances*, *6*(19), eaay7684. https://doi.org/10.1126/sciadv.aay7684

EC-Earth Consortium (EC-Earth). (2019). EC-Earth-Consortium ECEarth3-LR model output prepared for CMIP6 CMIP piControl,Version 20200409. *Earth System Grid Federation*. https://doi.org/10.22033/ESGF/CMIP6.4847

EC-Earth Consortium (EC-Earth). (2020). EC-Earth-Consortium ECEarth3-LR model output prepared for CMIP6 PMIP lig127k,Version 20200409. *Earth System Grid Federation*. https://doi.org/10.22033/ESGF/CMIP6.4798, 2020.

Gadgil, S., & Kumar, K. R. (2006). The Asian monsoon-agriculture and economy. In *The Asian Monsoon* (pp. 651–683). Berlin, Heidelberg: Springer.

Goswami, B. N., Venugopal, V., Sengupta, D., Madhusoodanan, M., & Xavier, P. K. (2006). Increasing trend of extreme rain events over India in a warming environment. *Science*, *314*(5804), 1442-1445. https://doi.org/1442-1445. 10.1126/science.1132027

Han, Z., Su, T., Zhang, Q., Wen, Q., & Feng, G. (2019). Thermodynamic and dynamic effects of increased moisture sources over the Tropical Indian Ocean in recent decades. *Climate Dynamics*, *53*(11), 7081–7096. https://doi.org/7081-7096. 10.1007/s00382-019-04977-w

Harrison, S. P., Bartlein, P., Izumi, K., Li, G., Annan, J., Hargreaves, J., et al. (2015). Evaluation of CMIP5 palaeo-simulations to improve climate projections. *Nature Climate Change*, *5*(8), 735-743. https://doi.org/10.1038/nclimate2649

Hazeleger, W., Severijns, C., Semmler, T., Stefanescu, S., Yang, S., Wang, X., et al. (2010). EC-earth: a seamless earth-system prediction approach in action. *Bulletin of the American Meteorological Society*, *91*(10), 1357-1363. https://doi.org/ 10.1175/2010BAMS2877.1

Hazeleger, W., Wang, X., Severijns, C., Ştefănescu, S., Bintanja, R., Sterl, A., et al. (2012). EC-Earth V2. 2: description and validation of a new seamless earth system prediction model. *Climate Dynamics*, *39*(11), 2611-2629. https://doi.org/10.1007/s00382-011-1228-5

Hirabayashi, Y., Mahendran, R., Koirala, S., Konoshima, L., Yamazaki, D., Watanabe, S., et al. (2013). Global flood risk under climate change. *Nature Climate Change*, *3*(9), 816-821. https://doi.org/10.1038/NCLIMATE1911

Hoffman, J. S., Clark, P. U., Parnell, A. C., & He, F. (2017). Regional and global sea-surface temperatures during the last interglaciation. *Science*, *355*(6322), 276-279. https://doi.org/10.1126/science.aai8464

Kageyama, M., Braconnot, P., Harrison, S. P., Haywood, A. M., Jungclaus, J. H., Otto-Bliesner, B. L., et al. (2018). The PMIP4 contribution to CMIP6–Part 1: Overview and over-arching analysis plan. *Geoscientific Model Development*, *11*(3), 1033-1057. https://doi.org/10.5194/gmd-11-1033-2018

Kathayat, G., Cheng, H., Sinha, A., Spötl, C., Edwards, R. L., Zhang, H., et al. (2016). Indian monsoon variability on millennial-orbital timescales. *Scientific Reports*, *6*(1), 1-7. https://doi.org/10.1038/srep24374

Kitoh, A., Endo, H., Krishna Kumar, K., Cavalcanti, I. F., Goswami, P., & Zhou, T. (2013). Monsoons in a changing world: A regional perspective in a global context. *Journal of Geophysical Research: Atmospheres*, *118*(8), 3053-3065. https://doi.org/10.1002/jgrd.50258

Lechleitner, F. A., Breitenbach, S. F., Rehfeld, K., Ridley, H. E., Asmerom, Y., Prufer, K. M., et al. (2017). Tropical rainfall over the last two millennia: evidence for a low-latitude hydrologic seesaw. *Scientific Reports*, *7*(1), 1-9. https://doi.org/10.1038/srep45809

Li, J., & Zeng, Q. (2000). Significance of the normalized seasonality of wind field and its rationality for characterizing the monsoon. *Science in China Series D: Earth Sciences*, *43*(6), 646-653. https://doi.org/10.1007/BF02879509

Li, J., & Zeng, Q. (2002). A unified monsoon index. *Geophysical Research Letters*, *29*(8), 1274. 10.1029/2001GL013874

Li, J., Wu, Z., Jiang, Z., & He, J. (2010). Can global warming strengthen the East Asian summer monsoon? *Journal of Climate*, *23*(24), 6696-6705. https://doi.org/10.1175/2010JCLI3434.1

Li, T. (2018). False amount effect—a discussion on one issue of isotopic climatology. *Quaternary Sciences*, *38*(6), 1545-1548. https://doi.org/10.11928/j.issn.1001-7410.2018.06.20

Liu, G., Li, X., Chiang, H.-W., Cheng, H., Yuan, S., Chawchai, S., et al. (2020). On the glacial-interglacial variability of the Asian monsoon in speleothem $\delta^{18}O$ records. *Science Advances*, *6*(7), eaay8189. https://doi.org/10.1126/sciadv.aay8189

Lunt, D. J., Abe-Ouchi, A., Bakker, P., Berger, A., Braconnot, P., Charbit, S., et al. (2013). A multi-model assessment of last interglacial temperatures. *Climate of the Past*, *9*(2), 699-717. https://doi.org/10.5194/cp-9-699-2013

Madec, G. (2008). NEMO reference manual, ocean dynamic component: NEMO-OPA. In *Note du Pôle modélisation, Inst. Pierre Simon Laplace, Fr.* (Tech. Rep., 27).

Magiera, M., Lechleitner, F. A., Erhardt, A. M., Hartland, A., Kwiecien, O., Cheng, H., et al. (2019). Local and regional Indian Summer Monsoon precipitation dynamics during Termination II and the Last Interglacial. *Geophysical Research Letters*, *46*(21), 12454-12463. https://doi.org/10.1029/2019GL083721

Midhun, M., Lekshmy, P., Ramesh, R., Yoshimura, K., Sandeep, K., Kumar, S., et al. (2018). The effect of monsoon circulation on the stable isotopic composition of rainfall. *Journal of Geophysical Research: Atmospheres*, *123*(10), 5205-5221. https://doi.org/10.1029/2017JD027427

Montoya, M., von Storch, H., & Crowley, T. J. (2000). Climate simulation for 125 kyr BP with a coupled ocean–atmosphere general circulation model. *Journal of Climate*, *13*(6), 1057-1072. https://doi.org/10.1175/1520-0442(2000)0132.0.CO;2

Nikolova, I., Yin, Q., Berger, A., Singh, U. K., & Karami, M. P. (2013). The last interglacial (Eemian) climate simulated by LOVECLIM and CCSM3. *Climate of the Past*, *9*(4), 1789-1806. https://doi.org/10.5194/cpd-8-5293-2012

Otto-Bliesner, B. L., Braconnot, P., Harrison, S. P., Lunt, D. J., Abe-Ouchi, A., Albani, S., et al. (2017). The PMIP4 contribution to CMIP6–Part 2: Two interglacials, scientific objective and experimental design for Holocene and Last Interglacial simulations. *Geoscientific Model Development*, *10*(11), 3979-4003. https://doi.org/10.5194/gmd-2016-279

Pedersen, R. A., Langen, P. L., & Vinther, B. M. (2017). The last interglacial climate: comparing direct and indirect impacts of insolation changes. *Climate Dynamics*, *48*(9), 3391-3407. https://doi.org/10.1007/s00382-016-3274-5

Ramesh, K., & Goswami, P. (2007). Reduction in temporal and spatial extent of the Indian summer monsoon. *Geophysical Research Letters*, *34*(23). https://doi.org/10.1029/2007GL031613

Roxy, M. K., Ritika, K., Terray, P., Murtugudde, R., Ashok, K., & Goswami, B. (2015). Drying of Indian subcontinent by rapid Indian Ocean warming and a weakening land-sea thermal gradient. *Nature communications*, *6*(1), 1-10. https://doi.org/10.1038/ncomms8423

Saha, A., Ghosh, S., Sahana, A.S., et al. (2014). Failure of CMIP5 climate models in simulating post-1950 decreasing trend of Indian monsoon. *Geophysical Research Letters*, *41*(20): 7323-7330. https://doi.org/10.1002/2014GL061573

Saji, N., Goswami, B., Vinayachandran, P., & Yamagata, T. (1999). A dipole mode in the tropical Indian Ocean. *Nature*, *401*(6751), 360-363. https://doi.org/10.1038/43854

Scussolini, P., Bakker, P., Guo, C., Stepanek, C., Zhang, Q., Braconnot, P., et al. (2019). Agreement between reconstructed and modeled boreal precipitation of the Last Interglacial. *Science Advances*, *5*(11), eaax7047. https://doi.org/10.1126/sciadv.aax7047

Singh, D., Tsiang, M., Rajaratnam, B., & Diffenbaugh, N. S. (2014). Observed changes in extreme wet and dry spells during the South Asian summer monsoon season. *Nature Climate Change*, *4*(6), 456-461. https://doi.org/10.1038/nclimate2208

Sinha, A., Kathayat, G., Cheng, H., Breitenbach, S. F., Berkelhammer, M., Mudelsee, M., et al. (2015). Trends and oscillations in the Indian summer monsoon rainfall over the last two millennia. *Nature Communications*, *6*(1), 1-8. https://doi.org/10.1038/ncomms7309

Sudharsan, N., Karmakar, S., Fowler, H. J., & Hari, V. (2020). Large-scale dynamics have greater role than thermodynamics in driving precipitation extremes over India. *Climate Dynamics*, *55*(9), 2603-2614. https://doi.org/10.1007/s00382-020-05410-3

Tan, M. (2014). Circulation effect: response of precipitation $\delta^{18}O$ to the ENSO cycle in monsoon regions of China. *Climate Dynamics*, *42*(3-4), 1067-1077. 10.1007/s00382-013-1732-x

Terray, P., Sooraj, K., Masson, S., & Prodhomme, C. (2021). Anatomy of the Indian Summer Monsoon and ENSO relationships in state-of-the-art CGCMs: Role of the tropical Indian Ocean. *Climate Dynamics*, *56*(1), 329-356. https://doi.org/10.1007/s00382-020-05484-z

Tokinaga, H., Xie, S.-P., Deser, C., Kosaka, Y., & Okumura, Y. M. (2012). Slowdown of the Walker circulation driven by tropical Indo-Pacific warming. *Nature*, *491*(7424), 439-443. https://doi.org/10.1038/nature11576

Turner, A. G., & Annamalai, H. (2012). Climate change and the South Asian summer monsoon. *Nature Climate Change*, *2*(8), 587-595. https://doi.org/10.1038/nclimate1495

Turney, C. S., & Jones, R. T. (2010). Does the Agulhas Current amplify global temperatures during super-interglacials? *Journal of Quaternary Science*, *25*(6), 839-843. https://doi.org/10.1002/jqs.1423

Turney, C. S., Jones, R. T., McKay, N. P., Van Sebille, E., Thomas, Z. A., Hillenbrand, C.-D., & Fogwill, C. J. (2020). A global mean sea surface temperature dataset for the Last Interglacial (129–116 ka) and contribution of thermal expansion to sea level change. *Earth System Science Data*, *12*(4), 3341-3356. https://doi.org/10.5194/essd-12-3341-2020

Vancoppenolle, M., Bouillon, S., Fichefet, T., Goosse, H., Lecomte, O., Morales Maqueda, M., & Madec, G. (2012). The Louvain-la-Neuve sea ice model. *Notes du pole de modélisation, Institut Pierre-Simon Laplace (IPSL)*. Paris, France.

Vittal, H., Karmakar, S., Ghosh, S., & Murtugudde, R. (2020). A comprehensive India-wide social vulnerability analysis: highlighting its influence on hydro-climatic risk. *Environmental Research Letters*, *15*(1), 014005. https://doi.org/10.1088/1748-9326/ab6499

Wang, B., Wu, Z., Li, J., Liu, J., Chang, C.-P., Ding, Y., & Wu, G. (2008). How to measure the strength of the East Asian summer monsoon. *Journal of Climate*, *21*(17), 4449-4463. https://doi.org/10.1175/2008JCLI2183.1

Wang, Y., Cheng, H., Edwards, R. L., Kong, X., Shao, X., Chen, S., et al. (2008). Millennial-and orbital-scale changes in the East Asian monsoon over the past 224,000 years. *Nature*, *451*(7182), 1090-1093. https://doi.org/10.1038/nature06692

Wu, G., Duan, A., Liu, Y., Mao, J., Ren, R., Bao, Q., et al. (2015). Tibetan Plateau climate dynamics: recent research progress and outlook. *National Science Review*, *2*(1), 100-116. https://doi.org/10.1093/nsr/nwu045

Wu, G., Liu, Y., He, B., Bao, Q., Duan, A., & Jin, F.-F. (2012). Thermal controls on the Asian summer monsoon. *Scientific Reports*, *2*(1), 1-7. https://doi.org/10.1038/srep00404

Zhang, Q., Berntell, E., Axelsson, J., Chen, J., Han, Z., de Nooijer, W., et al. (2021). Simulating the mid-Holocene, last interglacial and mid-Pliocene climate with EC-Earth3-LR. *Geoscientific Model Development*, *14*(2), 1147-1169. https://doi.org/10.5194/gmd-14-1147-2021

Zhang, Y., Li, J., Xue, J., Feng, J., Wang, Q., Xu, Y., et al. (2018). Impact of the South China Sea summer monsoon on the Indian Ocean dipole. *Journal of Climate*, *31*(16), 6557-6573. https://doi.org/10.1175/JCLI-D-17-0815.1